scientific reports

Check for updates

OPEN

Classification of melanoma skin Cancer based on Image Data Set using different neural networks

Rukhsar Sabir✉ & Tahir Mehmood

This paper aims to address the pressing issue of melanoma classification by leveraging advanced neural network models, specifically basic Convolutional Neural Networks (CNN), ResNet-18, and EfficientNet-B0. Our objectives encompass presenting and evaluating these models based on established practices in medical image diagnosis. Additionally, we aim to demonstrate their effectiveness in contributing to the critical task of saving lives through early and accurate melanoma diagnosis.Our methodology involves a multi-stage process, which includes image normalization and augmentation, followed by segmentation, feature extraction, and classification. Notably, the neural network models underwent rigorous evaluation, with EfficientNet-B0 exhibiting exceptional performance as the winning model. EfficientNet-B0 achieved a remarkable accuracy of 97%, surpassing ResNet-18 (87%) and basic CNN (80%) in classifying malignant and benign cases. In addition to accuracy, a comprehensive set of evaluation metrics was employed for EfficientNet-B0: sensitivity of 99%, specificity of 93%, F1-score of 97%, precision of 95%, and an error rate of 3%. It also demonstrated a Mathew's correlation coefficient of 94% and a geometric mean of 1.01. Across these metrics, EfficientNet-B0 consistently outperformed ResNet-18 and basic CNN. The findings from this research suggest that neural network models, particularly EfficientNet-B0, hold significant promise for precise and efficient melanoma skin cancer detection.

Melanoma, the most dangerous type of skin cancer in Australia and the fifth most prevalent in the UK, requires early detection in dermoscopy images to ensure effective treatment and cure[1,2]. Despite comprising only 4% of all skin cancers, melanoma accounts for a staggering 75% of skin cancer-related deaths, underscoring the critical need for early and accurate diagnostic methods[3]. Early detection is vital given melanoma's rapid spread and high growth rate, which predominantly affect the back, arms, legs, and face. Identifiable risk factors include UV light exposure, multiple moles, fair skin prone to quick burning, and a family history of the disease[4]. The traditional reliance on manual segmentation in medical imaging, while common, poses significant challenges, particularly the potential for bias introduced by subjective medical views[5]. This has spurred the advancement of automated and accurate diagnostic tools, which are crucial for improving outcomes in melanoma detection. Medical imaging, enhanced by technological advances, plays a pivotal role in the diagnosis and monitoring of skin conditions. However, as medical image analysis expands, challenges in organ segmentation and abnormality identification grow more complex[6].

In this context, neural networks, specifically Convolutional Neural Networks (CNNs), have proven effective in addressing image identification challenges and are increasingly applied in the medical domain[7]. Recent studies have demonstrated the potential of various neural network architectures in the classification of melanoma skin cancer (MSC) images. For instance, CNNs have been employed to explore the impact of varying the number of training images and epochs on classification accuracy[8]. Additionally, transfer learning architectures such as EfficientNet-B0 have shown remarkable success in network-based cancer detection, achieving high validation accuracy in tasks such as MRI-based tumor detection[9]. The effectiveness of CNN models, such as ResNet−18, has been well documented across various medical image datasets[10].

Several advanced methods have further demonstrated the effectiveness of CNNs in melanoma detection. Hybrid CNN models incorporating SVM classifiers have achieved notable accuracy in classifying dermoscopy images as benign or malignant lesions[11].Research has also shown the benefits of integrating image processing technologies with machine learning algorithms to enhance melanoma classification accuracy[12]. Additionally, approaches utilizing deep learning techniques and fusion of patient metadata have further advanced the classification of skin lesions[13–15]. Recent work by Ka et al. and Li Weipeng highlights the impact of combining feature extraction and metadata for improved skin condition classification[16,17].

School of Natural Sciences, National University of Science and Technology, Islamabad 46000, Pakistan. ✉email: rukhsarsabir17@gmail.com

Recent research by Kawahara et al. introduced the HierAttn network, which uses deep supervision and multi-branch attention mechanisms to enhance feature extraction and classification accuracy in skin lesions. This approach addresses limitations of traditional lightweight networks and achieves superior performance with a focus on practical implementation[18]. Similarly, the AIMIC platform provides a user-friendly, code-free interface for applying deep learning techniques to microscopic image classification, demonstrating high performance with ResNeXt−50−32d and MobileNet-V2. This platform is significant for making advanced deep learning accessible to users without programming expertise[19].

Building upon these developments, our research focuses on creating and assessing an MSC image classification system based on neural networks, including CNN, ResNet-18, and EfficientNet-B0. This approach not only leverages the strengths of advanced image processing technologies but also incorporates fine-tuning and transfer learning to enhance classification accuracy. Our findings suggest that these models can serve as non-invasive alternatives to traditional biopsy methods, providing high accuracy in the early detection of melanoma, which is critical for reducing the associated mortality rates[20–22]. Additionally, the recent study by M Suleman et al. presented the Smart MobiNet model, derived from MobileNet, to address the challenges of scalability, data availability, and diagnostic precision in melanoma detection. The model was evaluated on the ISIC 2019 dataset, demonstrating superior performance with an accuracy of 0.89 and balanced precision, sensitivity, and F1 scores of 0.90. This study emphasizes the importance of efficient and scalable models in real-world deployments, which aligns with the goals of our research[23].

Materials and methods

For melanoma skin cancer detection, we selected three neural network models: Convolutional Neural Networks (CNN), ResNet-18, and EfficientNet-B0. Each model was chosen based on its proven efficacy in medical image classification. The dataset shown in Fig. 1, carefully curated for its relevance to melanoma skin cancer classification, comprises binary classes distinguishing between benign and malignant cases.

Data availability

The dataset supporting the findings of this study is openly available in the Kaggle database refer to https://www.kaggle.com/datasets/hasnainjaved/melanoma-skin-cancer-dataset-of-10000-images as Melanoma Skin Cancer Dataset of 10,605 Images in this research. It comprises 9605 images designated for training the model and an additional 1000 images reserved for evaluating the model's performance. Each image in the dataset is standardized to the dimensions of 224 × 224 pixels and is represented in the RGB color scale.

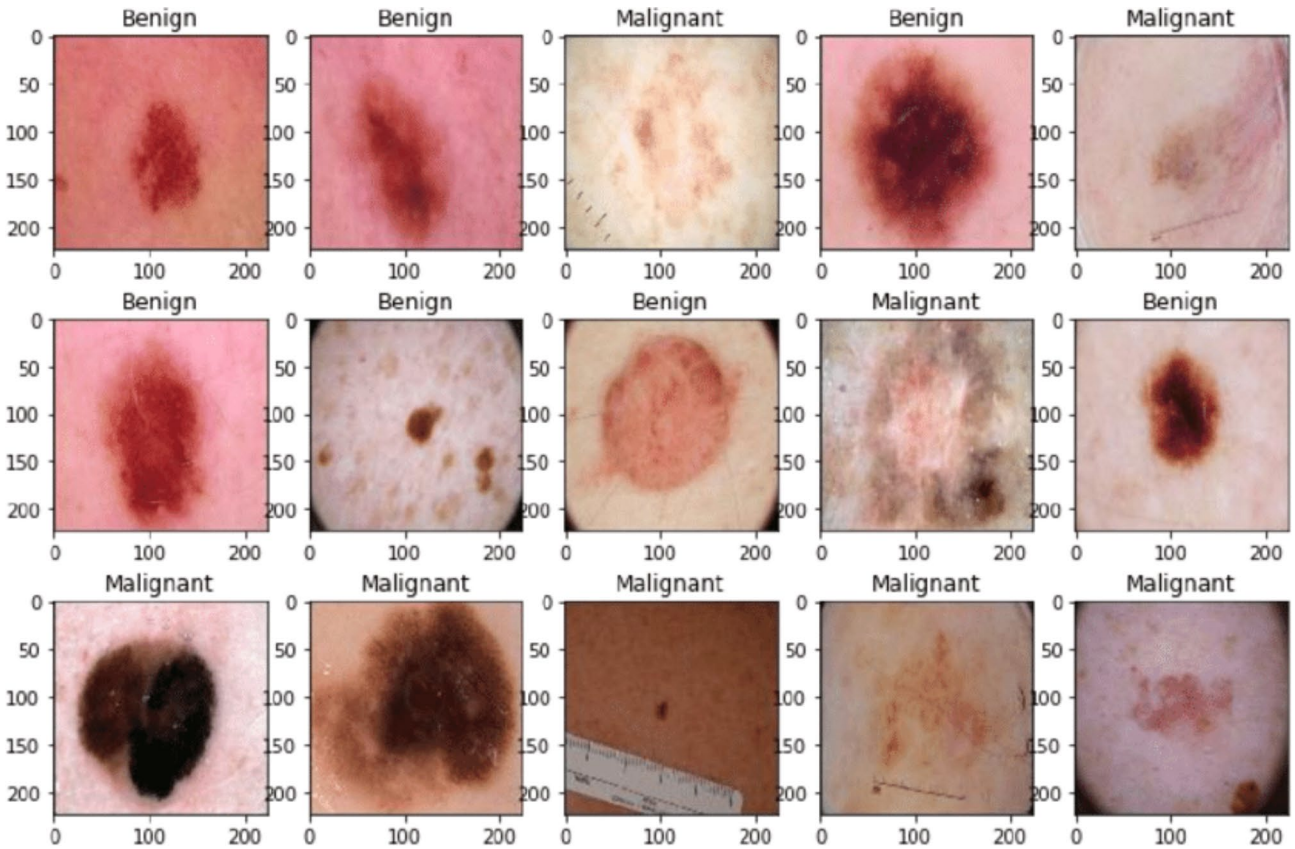

Fig. 1. This dataset comprises images classified into two categories: benign and malignant. These images are utilized both for training the model to learn distinguishing features and for testing its performance.

CNN

The CNN architecture for melanoma classification starts with a 224×224×3 input image of a skin lesion. The feature extraction process involves several convolutional layers using filters of various sizes (11×11, 5×5, 3×3) and strides, producing feature maps with dimensions such as 55×55×96 and 27×27×256. Max pooling layers reduce the spatial dimensions, for example, from 27×27×96 to 13×13×256. Residual blocks, which include skip connections, help train deeper networks. Further convolutional layers extract deeper features, maintaining or slightly reducing spatial dimensions, for example, to 13×13×384. The final max pooling layer reduces dimensions to 6×6×256, and flattening converts this to a 1D vector of 9216 elements. Fully connected layers process these features through layers with 4096 neurons, ultimately reducing to 1000 neurons for the final classification. The output layer produces a classification label indicating whether the lesion is melanoma or benign. This architecture effectively classifies melanoma skin cancer by progressively extracting and processing image features as shown in the CNN architecture in Fig. 2.

To assess the classification of melanoma skin cancer images, we used several key metrics. Accuracy measures the overall correctness of the model. Precision indicates the proportion of true melanoma cases among those predicted as melanoma, while Recall (or Sensitivity) assesses how well the model identifies all actual melanoma cases. Specificity evaluates the model's ability to correctly identify non-melanoma cases. The F1-Score balances Precision and Recall, and the Matthews Correlation Coefficient (MCC) provides a comprehensive view of the model's performance across all categories. The Geometric Mean reflects overall performance by considering both true positive and true negative rates. These metrics together offer a detailed evaluation of the model's effectiveness in classifying melanoma images.

ResNet-18

The ResNet-18 model for melanoma classification begins with an input image of a skin lesion shown in Fig. 3. The feature extraction process starts with multiple 3×3 convolutional layers, each followed by ReLU activation, producing initial feature maps of 112×112 dimensions. These layers are followed by several residual blocks, each containing convolutional layers and shortcut connections that help train deeper networks by allowing gradients to flow more effectively. The first residual block processes feature maps of size 112×112, the second block processes maps of size 56×56, the third block processes maps of size 26×26, and the fourth block processes maps of size 13×13. This hierarchical structure enables the network to capture increasingly complex features at each stage.

After the residual blocks, the network applies global average pooling, reducing the spatial dimensions of the feature maps. This is followed by two fully connected layers. The first fully connected layer has 4096 neurons, further processing the features, and the second fully connected layer has 10,000 neurons, preparing the final features for classification. The final output layer provides the classification label, indicating whether the input image is melanoma or benign. Figure 3; and Table 1 showcase the intricate feature extraction of this model.

EfficientNet-b0

The EfficientNet-B0 model for melanoma classification begins with an input image of a skin lesion. It starts with a 3×3 convolutional layer, combined with batch normalization (BN) and the Swish activation function,

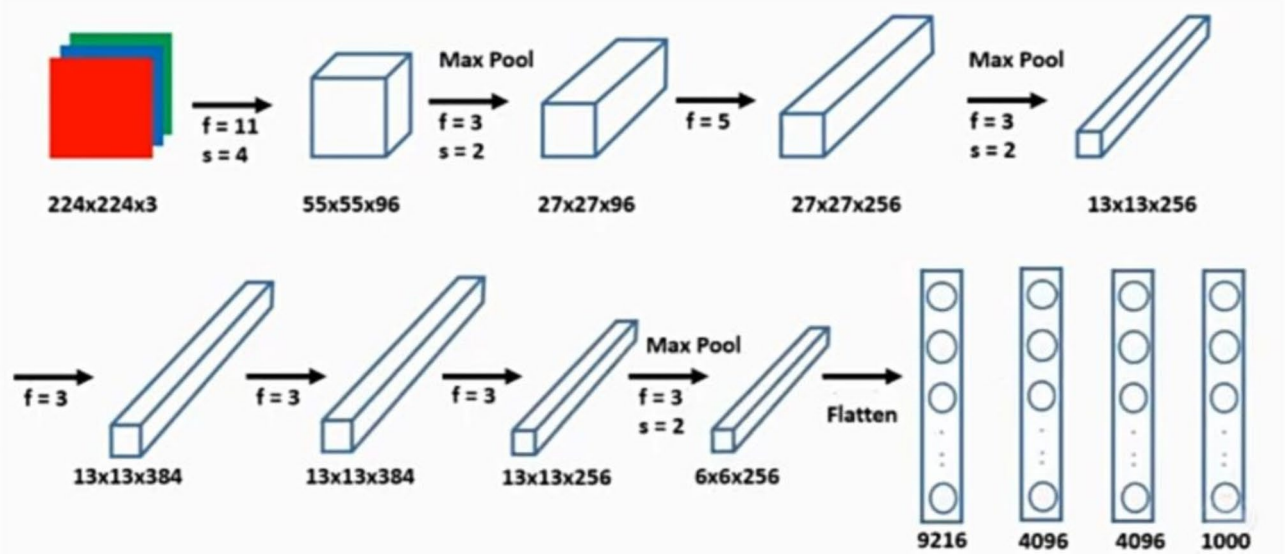

Fig. 2. This diagram illustrates the CNN (Convolutional Neural Network) model, highlighting the various layers that contribute to processing and extracting features from the skin cancer image dataset. Each layer in the CNN has a specific function: convolutional layers detect patterns and features, pooling layers reduce dimensionality and retain essential information, and fully connected layers combine features for classification.

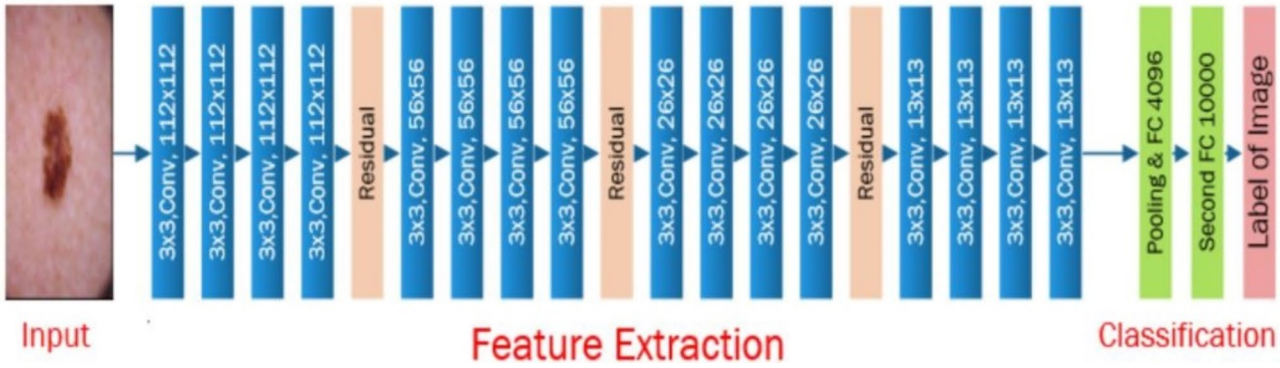

Fig. 3. This diagram outlines the foundational elements of the model, starting with convolutional layers, which are crucial for feature extraction from input data. It also includes batch normalization, which helps stabilize and accelerate the training process by normalizing activations.

Layer	Filter Size	Resolution	Activation Function
Input	-	224×224	-
Conv	3×3	112×112	Relu
Conv	3×3	112×112	Relu
Conv	3×3	112×112	Relu
Conv	3×3	112×112	Relu
Residual	-	112×112	-
Conv	3×3	56×56	Relu
Conv	3×3	56×56	Relu
Conv	3×3	56×56	Relu
Conv	3×3	56×56	Relu
Residual	-	56×56	-
Conv	3×3	26×26	Relu
Conv	3×3	26×26	Relu
Conv	3×3	26×26	Relu
Conv	3×3	26×26	Relu
Residual	-	26×26	-
Conv	3×3	13×13	Relu
Conv	3×3	13×13	Relu
Conv	3×3	13×13	Relu
Conv	3×3	13×13	Relu
Residual	-	13×13	-
Pooling and FC	-	4096	Relu
Second FC	-	10,000	Softmax

Table 1. This diagram illustrates the structure of the ResNet-18 model, focusing on its key components: convolutional layers and residual connections. The diagram shows how convolutional layers are used for feature extraction and how residual connections facilitate the training of deeper networks by allowing gradients to flow more easily through the network.

producing feature maps of dimensions 224×224×32. The model then proceeds through a series of mobile inverted bottleneck convolution (MBConv) blocks designed to capture features efficiently while minimizing computational cost.The first MBConv block processes the feature maps with dimensions 112×112×16 using 3×3 convolutions. The second MBConv block continues with 3×3 convolutions, producing feature maps of dimensions 112×112×24, followed by the third MBConv block that processes maps of 56×56×24. Subsequent MBConv blocks handle feature maps of sizes 56×56×40, 28×28×40, and 28×28×80, progressively downsampling the spatial dimensions while increasing the depth of the feature maps.

Further MBConv blocks process dimensions 14×14×80, 14×14×112, and finally 7×7×320, extracting increasingly complex features at each stage. After the MBConv blocks, a 3×3 convolution with batch normalization and Swish activation is applied, followed by a global average pooling layer that reduces the spatial dimensions to a 1D vector. The final step is a fully connected layer with softmax activation, which outputs the

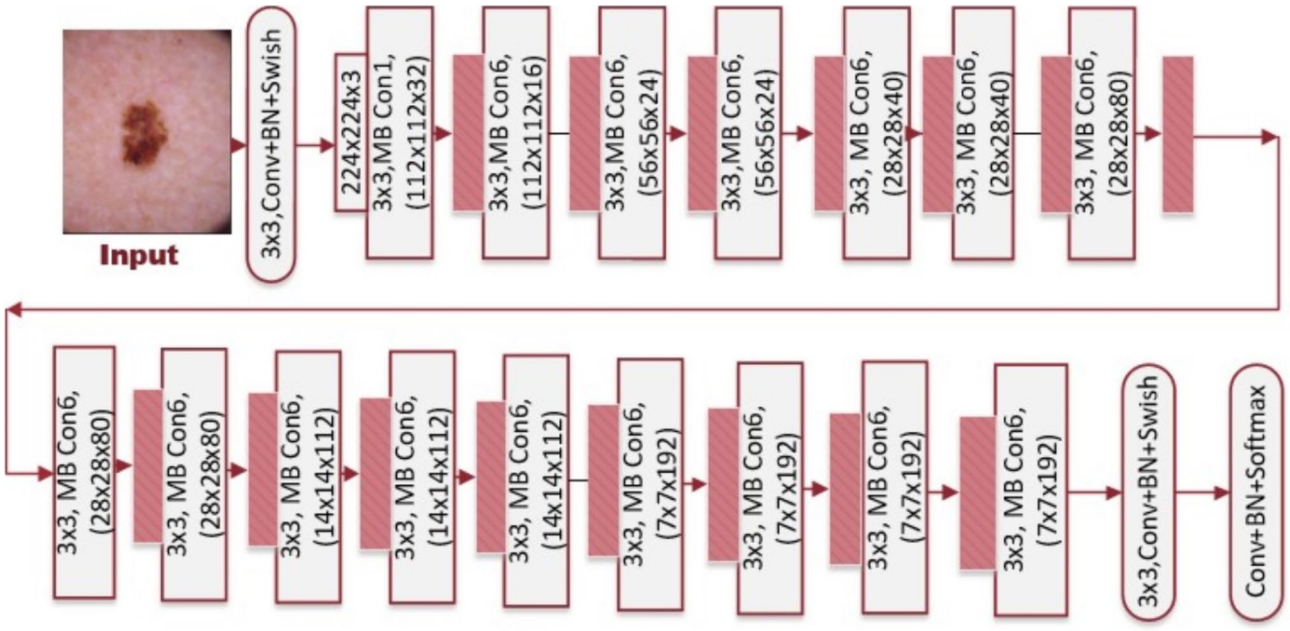

Fig. 4. This diagram provides an in-depth overview of the EfficientNet-B0 architecture. It includes key components such as filter sizes, image resolution, dimensions, and convolutional layers, offering a thorough understanding of the model's design.

Layer	Input	MBCon	MBCon	MBCon	MBCon	MBCon	MBCon	MBCon	Con	*P*-FC
Filter Size	-	3×3	3×3	3×3	3×3	3×3	3×3	3×3	1×1	-
Resolution	224×224	112×112	112×112	56×56	28×28	14×14	14×14	7×7	7×7	7×7

Table 2. This table provides a clear summary of the main features of the EfficientNet-B0 model, including details on filter sizes and image resolution. By examining these aspects, the table offers valuable insights into the model's design and its functional capabilities, helping to understand how these factors contribute to its performance.

classification label, indicating whether the lesion is melanoma or benign shown in Fig. 4 and expounded upon in Table 2.

Results and discussion

The collective exploration of skin cancer classification techniques encompasses a broad spectrum, ranging from traditional methods like PCA and SVM to advanced CNNs such as EfficientNet-B0, ResNet-50, and VGG-13, as well as hybrid CNNs. Across various studies, accuracy metrics varied from 75 to 93%, sensitivities from 52 to 95%, and specificities from 90 to 95%. Notably, EfficientNet-B0, ResNet-50, and spiking VGG-13 exhibited promise in detecting skin malignancies. The box plot shows in Fig. 5 compares the performance of three machine learning models CNN, ResNet-18, and EfficientNet-B0. EfficientNet-B0 stands out as the best performer, with the highest median accuracy and minimal variability, indicating it is highly effective and consistent in identifying melanoma cases. CNN also shows strong performance with a high median accuracy and a narrow IQR, suggesting stable and reliable results. In contrast, ResNet-18 has a lower median accuracy and a

wider interquartile range, reflecting greater variability and less reliability. This variability, coupled with the presence of outliers, suggests that ResNet-18 may not be as effective for this task without further adjustments.

EfficientNet-B0 is the top-performing model with an accuracy of 97%, outperforming CNN (80%) and ResNet-18 (87%). It excels in sensitivity (99%) and specificity (93%), demonstrating strong performance in identifying both positive and negative cases. With high precision (95%), an impressive F1-Score (97%), and the lowest error rate (0.03), EfficientNet-B0 is highly effective and reliable for skin cancer classification. It also boasts the highest Matthews Correlation Coefficient (94%) and Geometric Mean (1.01). CNN has the lowest Type-I error rate (4%), indicating a conservative approach with fewer false positives. EfficientNet-B0 and ResNet-18 have slightly higher Type-I error rates (6%). EfficientNet-B0 stands out with the lowest Type-II error rate (1%), suggesting it rarely misses actual melanoma cases. In comparison, CNN and ResNet-18 have higher Type-II error rates (3.6% and 1.8%, respectively). These findings highlight the balance between sensitivity and specificity in the models' performance. Our focused use of CNN, ResNet-18, and EfficientNet-B0 for melanoma skin cancer classification, as elucidated in Table 3.

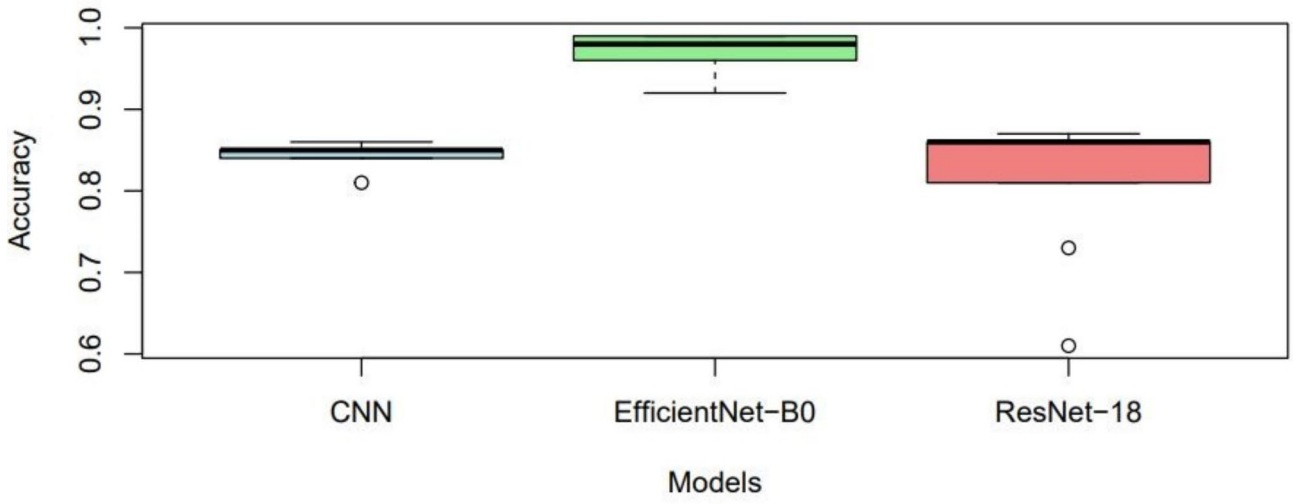

Fig. 5. This box plot compares the distribution of performance metrics for three different neural network models: CNN, ResNet-18, and EfficientNet-B0. The plot shows the median, quartiles, and any potential outliers in the performance scores, providing a visual summary of how each model performs.

Models	Accuracy	Sensitivity	Specificity	F1-Score	Precision	Error	MCC	GM	Type-I	Type-II
CNN	0.80	0.64	0.95	0.76	0.93	0.19	0.75	0.77	0.04	0.36
RNet-18	0.87	0.82	0.93	0.86	0.91	0.12	0.82	0.84	0.06	0.18
ENet-B0	0.97	0.99	0.93	0.97	0.95	0.03	0.94	1.01	0.06	0.01

Table 3. This table presents a summary of performance metrics for various neural network models applied to the melanoma skin cancer image dataset. Each metric reflects different aspects of model performance, such as its ability to correctly classify malignant versus benign cases and its overall reliability. By comparing these metrics, the table provides insights into the effectiveness and robustness of each model in classifying skin cancer, highlighting their strengths and potential areas for improvement.

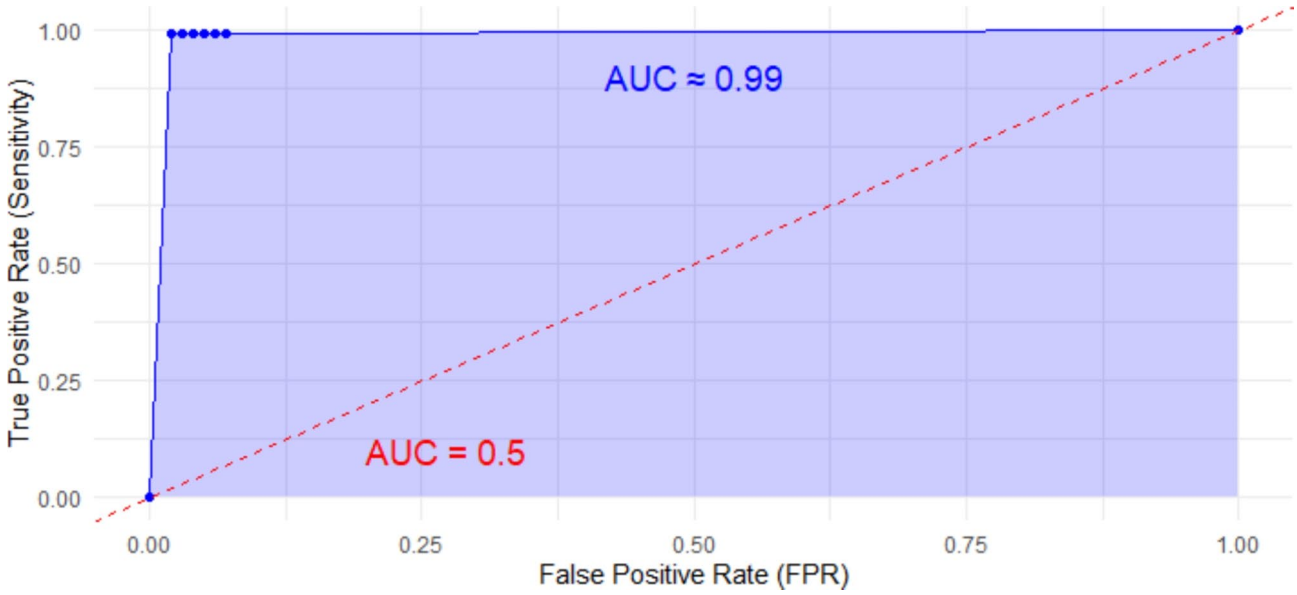

Fig. 6. This graph displays the ROC curves for each neural network model evaluated in the study. The ROC curves plot the True Positive Rate (sensitivity) on the y-axis against the False Positive Rate (1-specificity) on the x-axis. Each curve represents the trade-off between sensitivity and 1-specificity for a particular model, illustrating its ability to distinguish between malignant and benign cases.

Our investigation into the classification of melanoma images using CNN, ResNet-18, and EfficientNet-B0 has yielded valuable insights into the capabilities of these models. The comparison showcases a notable accuracy of 97% for EfficientNet- B0, outperforming both CNN (80%) and ResNet-18 (87%) in Fig. 7.The ROC curve for EfficientNet-B0 model in the melanoma skin cancer classification project shows exceptional performance in Fig. 7. It reveals a sensitivity of 99%, meaning the model successfully identifies nearly all melanoma cases, which is critical for early and accurate diagnosis. The curve also maintains a low False Positive Rate (FPR) across most thresholds, indicating that the model rarely misclassifies non-melanoma images.

as melanoma. This effectiveness in avoiding false positives highlights the model's reliability. The shape of the curve, rising sharply towards the top left and then leveling off, demonstrates that EfficientNet-B0 accurately distinguishes between melanoma and non-melanoma cases with minimal errors. The AUC value of approximately 0.99, close to 1.0, confirms nearly perfect classification performance. Positioned significantly above the random classifier's diagonal line (AUC = 0.5), the ROC curve indicates that EfficientNet-B0 significantly outperforms random guessing. Overall, the ROC curve and high AUC value reflect that EfficientNet-B0 excels in classifying melanoma skin cancer images with high sensitivity and low false positive rates.

In this study, EfficientNet-B0 emerged as the top-performing model, achieving an accuracy of 97%, significantly outperforming CNN (80%) and ResNet-18 (87%) shown in Fig. 7. Its superior performance can be attributed to its innovative architecture and the underlying principles that differentiate it from the more conventional CNN and ResNet-18 models. EfficientNet-B0 uses a compound scaling approach, which balances the network's width, depth, and resolution in a systematic and efficient manner. This method allows the model to utilize fewer resources while achieving higher accuracy. In contrast, CNN and ResNet-18 primarily scale by increasing either depth or width, which can lead to overfitting or computational inefficiency when dealing with large image datasets like the one used in this melanoma classification study. The compound scaling in EfficientNet-B0 results in an optimal network design that captures more features per layer while maintaining a manageable computational load. Moreover, EfficientNet-B0's use of depthwise separable convolutions allows it to reduce the number of parameters without compromising on feature extraction. This leads to lower computational overhead compared to ResNet-18, which relies on residual connections to address vanishing gradient problems, and CNN, which uses standard convolutional layers. While ResNet-18 is designed to tackle deeper network structures, it still lacks the parameter efficiency that EfficientNet-B0 achieves through its architecture. Additionally, the use of squeeze-and-excitation blocks in EfficientNet-B0 enhances its ability to focus on the most relevant features by recalibrating channel-wise feature responses. This feature is absent in both CNN and ResNet-18, which may explain why EfficientNet-B0 demonstrates higher sensitivity (99%) and specificity (93%). These recalibration blocks enable the model to prioritize important patterns, particularly useful in detecting subtle differences between melanoma and non-melanoma images. The results indicate that EfficientNet-B0 is highly efficient in both computational resources and performance metrics, making it a superior model for skin cancer classification. Its balanced approach to scaling, along with advanced architectural enhancements, enables it to outperform traditional models like CNN and ResNet-18 in identifying melanoma with higher precision, F1-score, and lower error rates.

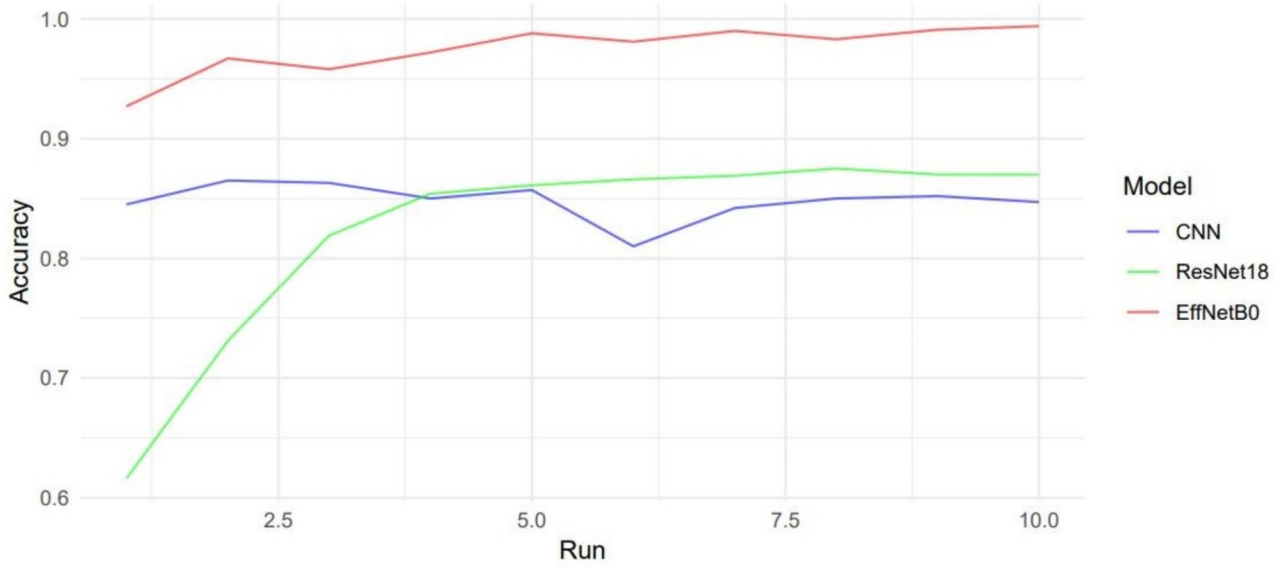

Fig. 7. This graph uses three different colors to display the model accuracy for each method. The number of epochs is displayed on the horizontal axis, and the vertical axis measures model accuracy. ResNet18 and CNN are represented by the blue and green lines, and the yellow line shows the EfficientNet-B0 method.

Conclusion

The study titled "Classification of Melanoma Skin Cancer Using Deep Learning" demonstrates the remarkable potential of advanced neural network models in the early and accurate diagnosis of melanoma. Our comprehensive evaluation indicates that EfficientNet-B0 significantly outperforms both ResNet-18 and basic CNN models across multiple metrics. EfficientNet-B0 achieved an accuracy of 97%, sensitivity of 99%, specificity of 93%, F1-score of 97%, precision of 95%, and an error rate of 3%. Additionally, it demonstrated a Mathew's correlation coefficient of 94% and a geometric mean of 1.01. Across these metrics, EfficientNet-B0 consistently surpassed the performance of ResNet-18, which achieved an accuracy of 87%, and basic CNN, which achieved an accuracy of 80%. These findings underscore the critical role of EfficientNet-B0 in enhancing melanoma detection and highlight its promise as a valuable tool in medical diagnostics, potentially contributing to improved patient outcomes through timely and precise cancer detection.

Data availability

The dataset supporting the findings of this study is openly available in the Kaggle database at [https://www.kaggle.com/datasets/hasnainjaved/melanoma-skin-cancer-dataset-of-10000-images], referenced as Melanoma Skin Cancer Dataset of 10000 Images in this research. This dataset was used under the conditions provided by Kaggle's terms of service for academic research purposes. Any further inquiries can be directed to the corresponding author.

Received: 22 April 2024; Accepted: 3 October 2024
Published online: 29 November 2024

References

1. Sheha, M. A. et al. Automatic detection of melanoma skin cancer using texture analysis. *Int. J. Comput. Appl.* **42**, 22–26 (2012).
2. Eltayef, K., Li, Y. & Liu, X. Detection of melanoma skin cancer in dermoscopy images. In *Journal of physics: conference series*, vol. 787, 012034IOP Publishing, (2017).
3. Jain, S. et al. Computer aided melanoma skin cancer detection using image processing. *Procedia Comput. Sci.***48**, 735–740 (2015).
4. Jaleel, J. A., Salim, S. & Aswin, R. B. Computer aided detection of skin cancer. In *International Conference on Circuits, Power and Computing Technologies (ICCPCT)*, 1137–1142, DOI: (2013). https://doi.org/10.1109/ICCPCT.2013.6528879 (2013).
5. Yin, X. X. et al. U-net-based medical image segmentation. *J. Healthc. Eng.* (2022). (2022).
6. Malhotra, P. et al. Deep neural networks for medical image segmentation. *J. Healthc. Eng.* (2022). (2022).
7. Dhruv, P. & Naskar, S. Image classification using convolutional neural network (cnn) and recurrent neural network (rnn): A review. *Mach. Learn. Inf. Process. Proc. ICMLIP 2019* 367–381 (2020).
8. Refianti, R., Mutiara, A. B. & Priyandini, R. P. Classification of melanoma skin cancer using convolutional neural network. *Int. J. Adv. Comput. Sci. Appl.***10** (2019).
9. Shah, H. A. et al. A robust approach for brain tumor detection in magnetic resonance images using finetuned efficientnet. *IEEE Access.***10**, 65426–65438 (2022).
10. Sarwinda, D., Paradisa, R. H., Bustamam, A. & Anggia, P. Deep learning in image classification using residual network (resnet) variants for detection of colorectal cancer. *Procedia Comput. Sci.***179**, 423–431 (2021).
11. Keerthana, D., Venugopal, V., Nath, M. K. & Mishra, M. Hybrid convolutional neural networks with svm classifier for classification of skin cancer. *Biomed. Eng. Adv.***5**, 100069 (2023).
12. Mhaske, H. & Phalke, D. Melanoma skin cancer detection and classification based on supervised and unsupervised learning. In *2013 international conference on Circuits, Controls and Communications (CCUBE)*, 1–5IEEE, (2013).
13. Zghal, N. S. & Derbel, N. Melanoma skin cancer detection based on image processing. *Curr. Med. Imaging.* **16**, 50–58 (2020).
14. Bonechi, S. et al. Fusion of visual and anamnestic data for the classification of skin lesions with deep learning. In *New Trends in Image Analysis and Processing–ICIAP 2019: ICIAP International Workshops, BioFor, PatReCH, e-BADLE, DeepRetail, and Industrial Session, Trento, Italy, September 9–10*, Revised Selected Papers 20, 211–219 (Springer, 2019). (2019).
15. Gessert, N., Nielsen, M., Shaikh, M., Werner, R. & Schlaefer, A. Skin lesion classification using ensembles of multi- resolution efficientnets with meta data. *MethodsX.* **7**, 100864 (2020).
16. Kawahara, J., Daneshvar, S., Argenziano, G. & Hamarneh, G. Seven-point checklist and skin lesion classification using multitask multimodal neural nets. *IEEE J. Biomedical Health Inf.***23**, 538–546 (2018).
17. Li, W., Zhuang, J., Wang, R., Zhang, J. & Zheng, W. S. Fusing metadata and dermoscopy images for skin disease diagnosis. In *2020 IEEE 17th international symposium on biomedical imaging (ISBI)*, 1996–2000 (IEEE, 2020).
18. Dai, W. et al. Deeply supervised skin lesions diagnosis with stage and branch attention. *IEEE J. Biomed. Heal Inf.* (2023).
19. Liu, R. et al. Aimic: deep learning for microscopic image classification. *Comput. Methods Programs Biomed.***226**, 107162 (2022).
20. Ali, K., Shaikh, Z. A., Khan, A. A. & Laghari, A. A. Multiclass skin cancer classification using efficientnets–a first step towards preventing skin cancer. *Neurosci. Inf.***2**, 100034 (2022).
21. Elgamal, M. Automatic skin cancer images classification. *Int. J. Adv. Comput. Sci. Appl.***4** (2013).
22. Yap, J., Yolland, W. & Tschandl, P. Multimodal skin lesion classification using deep learning. *Exp. Dermatology*. **27**, 1261–1267 (2018).
23. Suleman, M. et al. Smart mobinet: a deep learning approach for accurate skin cancer diagnosis. *CMC-COMPUTERS Mater. CONTINUA*. **77**, 3533–3549 (2023).

Acknowledgements

This research is not just a reflection of my academic endeavor, but also a tribute to the enduring love and support of my family and friends. Most profoundly, I dedicate this work to my late father, Muhammad Sabir. As his only child, I was blessed with his undivided love, wisdom, and encouragement. He taught me that with perseverance and faith, no obstacle is too great to overcome. His absence is deeply felt, but his spirit continues to guide and inspire me daily. This achievement is a tribute to his cherished memory, forever a source of light and inspiration in my life.

Author contributions

Rukhsar Sabir led the research from conception to completion. She was responsible for designing the study, conducting the experiments, and analyzing the data, and critically assessing the results, contributing to the

project's key findings.Tahir Mehmood, as supervisor, provided essential guidance and mentorship throughout the research process. His expertise was invaluable in shaping the research objectives, offering methodological insights, thereby enriching the intellectual depth and clarity of the manuscript.

Declarations

Competing interests

The authors declare no competing interests.

Additional information

Correspondence and requests for materials should be addressed to R.S.

Reprints and permissions information is available at www.nature.com/reprints.

Publisher's note Springer Nature remains neutral with regard to jurisdictional claims in published maps and institutional affiliations.